

Imaging Ectopic Fat Deposition in *Caenorhabditis Elegans* Muscles Using Nonlinear Microscopy

MEROPI MARI,^{1,2} GEORGE FILIPPIDIS,^{1*} KONSTANTINOS PALIKARAS,² BARBARA PETANIDOU,^{1,3} COSTAS FOTAKIS,^{1,3} AND NEKTARIOS TAVERNARAKIS^{2,4}

¹Institute of Electronic Structure and Laser, Foundation for Research and Technology, Heraklion, Crete 71110, Greece

²Institute of Molecular Biology and Biotechnology, Foundation for Research and Technology, Heraklion, Crete 71110, Greece

³Physics Department, University of Crete, Heraklion, Crete 71003, Greece

⁴Medical School, University of Crete, Heraklion, Crete 71003, Greece

KEY WORDS THG; SHG; nonlinear phenomena; imaging; *C. elegans*; ectopic fat accumulation

ABSTRACT The elucidation of the molecular mechanisms that lead to the development of metabolic syndrome, a complex of pathological conditions including type-2 diabetes, hypertension, and cardiovascular diseases, is an important issue with high biological significance and requires accurate methods capable of monitoring lipid storage distribution and dynamics in vivo. In this study, the nonlinear phenomena of second and third harmonic generation (SHG, THG) have been employed simultaneously as label-free, nondestructive diagnostic techniques, for the monitoring and the complementary three-dimensional (3D) imaging and analysis of the muscular areas and the lipid content localization. THG microscopy was used as a quantitative tool in order to record the accumulation of lipids in nonadipose tissues in the pharyngeal muscles of 18 *Caenorhabditis elegans* (*C. elegans*) specimens, while the SHG imaging provided the detailed anatomical information about the structure of the muscles. The ectopic accumulation of fat on the pharyngeal muscles increases in wild-type (N2) *C. elegans* between 1 and 9 days of adulthood. This suggests a correlation of ectopic fat accumulation with the process of aging. Our results can contribute to the unraveling of the link between the deposition of ectopic fat and aging, but mainly to the validation of SHG and THG microscopy modalities as new, noninvasive tools to localize and quantify selectively lipid formation and distribution. *Microsc. Res. Tech.* 78:523–528, 2015. © 2015 Wiley Periodicals, Inc.

INTRODUCTION

The development of innovative microscopy techniques in combination with protein labels specific for lipids has accelerated the studies on lipid research. Most research on lipid storage has been relied on biochemical investigation (Brooks et al., 2009; Mak et al., 2006). Some traditional biochemical techniques used are gas chromatography (Watts and Browse, 2002) or thin-layer chromatography (TLC) (Watts and Browse, 2006). However, biochemical methods require a large number of *C. elegans* and lack of spatial information upon analysis on the whole animals.

There is an arsenal of fluorescent-based techniques used to the study of lipid metabolism. Fixation and staining or fluorescence imaging of live worms through dye feeding are the most popular fluorescent-based methods, while Nile Red (Greenspan and Fowler, 1985), BODIPY (Mak et al., 2006), and Sudan black (Ashrafi et al., 2003) are the most common and efficient lipid stains widely used. Nevertheless, there is a need for fast, noninvasive, label-free microscopy methods to achieve lipid content imaging and quantification.

Coherent anti-Stokes Raman scattering (CARS) microscopy has been used to monitor *C. elegans* lipid profile (Hellerer et al., 2007). This is a method that

allows lipid imaging without the need of staining techniques. In wild-type animals, the labeled fat corresponded well to the lipids imaged by CARS. CARS measurements are not background-free, due to the strong autofluorescence and the nonresonant signal arising from any objects or surrounding solvent. These drawbacks limit the image contrast and spectral selectivity of the technique (Cheng and Xie, 2004). In addition, this technique is valuable and efficient due to its chemical specificity, but it is costly as it requires two tightly synchronized and perfectly aligned laser beams (Potma et al., 2002). Similarly with CARS, stimulated Raman scattering (SRS) is based on the chemical contrast of intrinsic Raman vibrational frequencies

*Correspondence to: George Filippidis; Institute of Electronic Structure and Laser, Foundation for Research and Technology, Heraklion 71110, Crete, Greece. E-mail: fillip@iesl.forth.gr

Received 28 January 2015; accepted in revised form 22 March 2015

REVIEW EDITOR: Prof. Alberto Diaspro

Contract grant sponsor: FP7 Projects “LASERLAB-EUROPE”; Contract grant number: 228334; Contract grant sponsor: REGPOT-2012-2013-1 and The BIOSYS Research Project, Action KRIPIS; Contract grant number: MIS-448301 (2013SE01380036); Contract grant sponsor: General Secretariat for Research and Technology, Ministry of Education, Greece and the European Regional Development Fund (Sectoral Operational Programme: Competitiveness and Entrepreneurship, NSRF 2007-2013)/European Commission.

DOI 10.1002/jemt.22504

Published online 20 April 2015 in Wiley Online Library (wileyonlinelibrary.com).

contributing to better quality images free of nonresonant background. SRS was performed to record the fat storage of *C. elegans* mutants, providing valuable knowledge on genes regulating fat metabolism (Wang et al., 2011). The proper tuning of two synchronized beams is required for the realization of the SRS measurements (Lu et al., 2012).

SHG and THG are coherent nonlinear scattering phenomena. SHG signal is produced from noncentrosymmetric molecules and provides information, which is related to structures with high degree of orientation and organization but without inversion symmetry (Pelagati et al., 2012). These structures in tissues are myosin thick filaments (Cox et al., 2003), collagen (Rehnberg et al., 2011), microtubules (Dombeck et al., 2003), or lipid membranes (Zhuo et al., 2012).

On the other hand, THG is sensitive to local differences in third-order nonlinear susceptibility $\chi^{(3)}$, refractive index, and dispersion. Under tight focusing conditions, the extent of THG signal increases dramatically when the beam focus spans an interface between two optically different materials.

THG is a powerful noninvasive imaging technique capable of revealing the anatomic features of many model organisms such as *C. elegans* in vivo (Gualda et al., 2008). THG requires a single beam and has already proven its efficiency to monitor cellular processes in vivo (Filippidis et al., 2009), but also in vitro combined with other nonlinear modalities (Aptel et al., 2010).

Recent studies have shown that THG is able of visualizing the morphology of unstained tissues (Oron et al., 2004; Witte et al., 2011) as well as lipid bodies in tissues and cells (Débarre et al., 2006; Zimmerley et al., 2013). THG imaging has characterized different developmental stages of the nematode *C. elegans* (Aviles-Espinosa et al., 2010; Tserevelakis et al., 2010) and has recorded in time the progress of the embryonic development (Olivier et al., 2010; Tserevelakis et al., 2011). Furthermore, THG imaging is capable of providing valuable information concerning the energetic status of preimplantation mouse embryos and blastomere equivalence, by detecting lipid body structures (Kyvelidou et al., 2011). Moreover, THG has been previously presented to visualize successfully intestinal lipid droplets (adipose tissue) in *C. elegans*, while Two Photon Excitation Fluorescence (TPEF) was used to confirm the efficient THG imaging of stained lipids with various labels (Tserevelakis et al., 2014).

In this study, THG imaging microscopy has been used as diagnostic tool for the detection and quantification of ectopic accumulation of lipids in non-adipose tissues (pharyngeal muscles). We have utilized the nematode worm *C. elegans* which has emerged as a versatile model organism (Vancoppenolle et al., 2000) for our studies.

MATERIALS AND METHODS

C. elegans: Strains and Maintenance

We followed standard procedures for *C. elegans* maintenance. Briefly, worms were kept at 20°C and maintained on standard NGM plates seeded with *E. coli* OP50 bacteria. Bristol N2: wild-type strain used in the study.

Lipid Staining

NGM plates were seeded with OP50 *E. coli* bacteria and allowed to dry overnight at room temperature. L4-stage worms were incubated on plates seeded with OP50 bacteria and transferred to fresh plates every other day until they reached day 1 and day 9 of adulthood.

For Nile Red staining: Prior to viewing, worms were fixed for 5 min in 3 mL cold (−20°C) methanol. Subsequently, 2 mL of PBTw (PBS with 0.1% Tween-20) were added, and tubes were centrifuged for 2 min at 3000 rpm to remove the supernatant. Finally, worms were washed twice in PBTw. Following fixation, worms were stained for 20 min in 10 mM Nile Red (Sigma-Aldrich Corp.), added from a stock solution of 50 mM Nile Red diluted in 100% ethanol.

For second and third harmonic generation imaging microscopy: Prior to viewing, worms were collected with M9 isotonic buffer (22 mM KH_2PO_4 (Merck cat. no. 1.04873.1000), 42 mM Na_2HPO_4 (Merck cat. no. 1.06586.0500), 85 mM NaCl (Merck cat. no. 1.06404.1000), and 1 mM MgSO_4 (Sigma cat. no. M-7506). Dissolve 3 g KH_2PO_4 , 6 g Na_2HPO_4 , 5 g NaCl, and 1 m: 1 M MgSO_4 in 1 L distilled water. Autoclave and keep it refrigerated). Then, worms were washed several times with M9 buffer to remove bacteria. Finally, the worms were immobilized with 10 mM sodium azide buffer at final concentration. Finally, immobilization worms are examined microscopically.

Experimental Apparatus

The experimental set up was similar to the one described in our previous studies (Tserevelakis et al., 2011; Tserevelakis et al., 2014). It consists of a t-pulse femtosecond laser (Amplitude systems, 1028 nm, 50 MHz, 1 W, 200 fs) that has been used as an excitation source. A modified Nikon upright microscope (Eclipse ME600D) is employed. Adjustable neutral density filters (New Focus, Newport Corp.) are utilized to control the power at the sample plane. A set of galvanometric mirrors (Cambridge Technology) is placed on the microscope and allows the sample scanning. A telescope system is used to control the beam radius. It is important to control the beam diameter in order to fulfill the back aperture of the objective lens so that the maximum field of view and the tight focusing within the limits of the lens are achieved and no power is lost. The focal plane is selected by using a motorized translation stage (Standa Ltd., Lithuania; 1 μm minimum step). The beam is tightly focused on the sample plane by using objective lens of high numerical aperture (Carl Zeiss, C-Achroplan 32x, NA 0.85, water immersion). Specimens are placed between two very thin ($\sim 70 \mu\text{m}$) glass coverslips. A 35 mm diameter circular coverslips of 0.06–0.08 mm thickness were employed (Marienfeld, Germany, cat.no.011972039 159). This is the thinnest glass coverslips found in the market, which transmits a satisfactory amount of 343 nm THG signal. The objective used contains an aberration correction ring that is appropriate for any glass coverslip thickness between 0–0.17 mm. The glass slides are separated by a 100 μm spacer in order to protect the specimens. A condenser lens (Carl Zeiss, PlanNeofluar, 40x, 0.75 NA, air immersion) collects

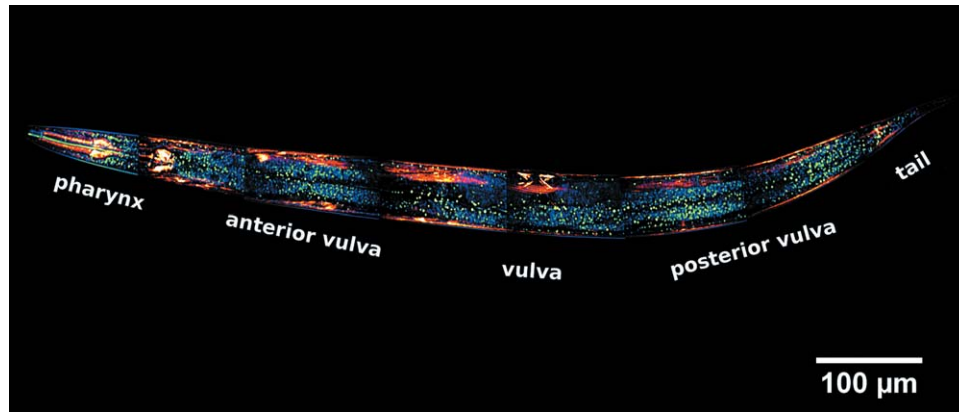


Fig. 1. Complementary nonlinear imaging of the whole body of 1-day-old adult *C. elegans*. THG (green blue) visualizes the intracellular compartments such as lipids, lumen, cuticle, and SHG (red hot) reveals the musculature of the animal. [Color figure can be viewed in the online issue, which is available at www.interscience.wiley.com.]

the THG signals in the transmission mode. Our apparatus contains an objective and a condenser lens of a similar N.A. The main reason is that this particular condenser presents a higher transmission of the UV light (343 nm) of the THG signal. In addition, its working distance is appropriate for our setup. For our statistics, THG is detected in the forward path, while SHG is detected in the backscattered direction. Thus, any loss (due to the N.A. of the condenser) of SHG signal is avoided.

The two nonlinear signals (THG and TPEF or SHG) that are simultaneously generated into the focal volume are collected in the transmission and the reflection mode, respectively. This quality of our system makes it capable of performing colocalization measurements. Sample scanning and data acquisition are controlled through a LabVIEW interface, adapted to the experiment requirements. A CCD camera (PixeLINK) is used for observation. The signals of the reflection mode (SHG or TPEF) are recorded by a photomultiplier tube (PMT; Hamamatsu) that is attached on the microscope eyepiece site and wired to the computer. Appropriate filters are placed in front of the PMT to cut off the reflected laser beam but also to collect the TPEF or SHG signals. Specifically, for the TPEF measurements, a short pass filter (SPF 700 nm, CVI) was placed at the PMT input to cut off any reflection from the laser beam and a bandpass filter (640 nm/40 nm, Chroma), which eliminates any SHG reflection. For SHG, a 514 nm bandpass filter (CVI F03-514.5) was used. A colored glass filter (U 340-Hoya) is placed in front of the second PMT (Hamamatsu) for the detection of the THG signals. The laser power on the sample plane was 48 mW for all measurements (~ 1 nJ per pulse).

For this presented work, the 500×500 pixel images of all modalities are averaged 30 times to improve the signal to noise ratio. The total acquisition time for each image was 33 seconds. All the figures are z-projections of slice images separated by a $2 \mu\text{m}$ distance. For all the figures, the pixel size is $0.27 \mu\text{m}$. For the reconstruction and processing of the figures, Image J was employed (NIH, <http://imagej.nih.gov/ij/>).

RESULTS AND DISCUSSION

THG comprises an ideal diagnostic tool that gives unique morphological information for various samples. Furthermore, lipid depositions in tissues are prominent third harmonic generating sources (Débarre et al., 2006). In combination with SHG, complementary information on the musculature but also internal structures can be extracted. Previous work (Tserevelakis et al., 2014) has shown that the visualization of adipose fat in the intestine region of *C. elegans* samples is feasible by employing THG microscopy. In this study, we focus on nonadipose tissues of the worm (pharyngeal muscles) in order to quantify precisely the ectopic fat accumulation by using non-destructive, label-free imaging techniques.

Figure 1 reveals the anatomic features of the whole body of 1-day-old adult wild-type *C. elegans* via the simultaneous performance of THG and SHG measurements. It is the first time to our knowledge, where the whole body of *C. elegans* is sequentially recorded in high resolution and imaged by using the label free nonlinear phenomena of THG and SHG. THG reveals the contour, shape, and internal structures of the animal (green blue), while the musculature (red hot) is revealed by SHG. Specifically, SHG imaging provides anatomical information for the body wall muscles, the two pharyngeal bulbs, the striated muscles in the mid-body region, the vulva, and the muscles located in the posterior part of the worm. Figure 1 is a montage of eight three-dimensional z-projected stacks, which consist of different number of slices. It consists of eight sequential scans each of which is composed of z-projections of 21 slices at the head region, 29 slices in the middle area around the vulva, and 13 slices at the tail region. The different areas are selected manually by choosing the proper x-y values in the motorized stage. The shading effect in Figure 1 is due to the uneven illumination effect that results in the fading of the signal at the edges of the image and a slight sample movement.

In order to identify the lipid content of the *C. elegans* and exclude any other cellular structures that give rise

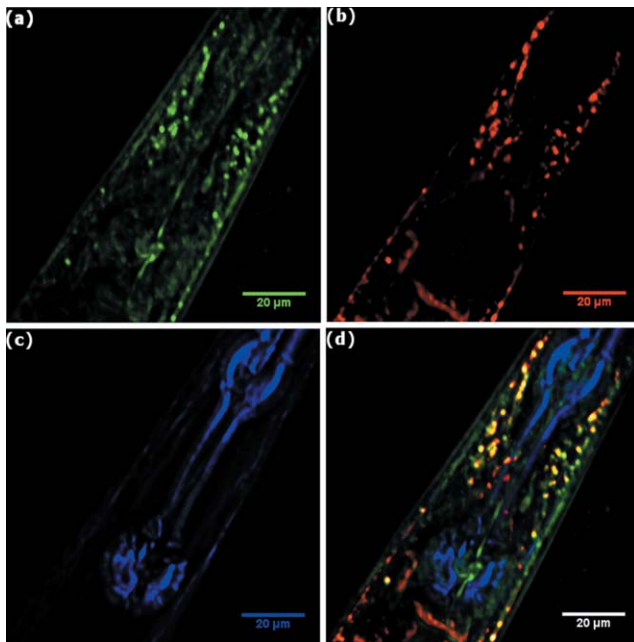


Fig. 2. The three-color images of the head area of a 1-day-old stained adult *C. elegans*. (a) THG (green) arises from internal head structures (mostly lipids), (b) TPEF (red) emanating from the lipids stained with Nile Red, (c) SHG (purple) originating from the musculature of the head region (pharyngeal and body wall muscles), and (d) the merge of all three colors. [Color figure can be viewed in the online issue, which is available at wileyonlinelibrary.com.]

to THG signal, Nile Red was used to specifically stain the lipids of the animals. Simultaneous measurements of THG and TPEF were performed on the pharynx of *C. elegans* to confirm the colocalization of TPEF with THG signals. We investigate the feasibility of THG to localize the ectopic fat accumulation on muscle cells. Whereas *C. elegans* lacks of dedicated adipose tissues, its intestine and hypodermis serve as the main lipid storage sites. The head region and especially the area between the two bulbs of the pharynx is the only part of the animal where the intestinal lipids are excluded. This is critical for the following measurements of the THG signal quantification that has to exclude any signal coming from the adipose tissue.

Figure 2d is a merge of the three color signals; (a) THG in green, (b) TPEF in red, and (c) SHG in purple. The contour, the shape, the linings of the animal pseudocoelomic cavity, and other discontinuities in the anterior body segment are detected through THG measurements. Moreover, high THG signals arise from structures (mainly lipids) that their third-order susceptibility values vary significantly from the surrounding media (Fig. 2a). Figure 2b depicts the TPEF from Nile Red that labels the lipid droplets in fixed animals. Figure 2c presents the SHG imaging (purple) emanating from the musculature of the head region (pharyngeal and body wall muscles). In this case, SHG signals were recorded in the transmission mode. Figure 2d is the merge of the three nonlinear signals. Figure 2d depicts the colocalization of the TPEF (red), arising from the stained lipid droplets, with the THG (green) originating from the internal circular structures of the head, which are mainly lipids. However,

THG signals arise from various discontinuities in the anterior part of the animal. In Figure 2d, it is shown that the lipids of the head muscles are revealed by THG (green) and colocalized with TPEF (red) resulting in the yellow structures. These components indicate the ectopic fat in the head region of the animal. Nile Red has stained all the lipid structures, even the ones of the intestine (under the second bulb of the pharynx) which are not of our interest. The fluorescence might be more intense compared to the THG on some structures resulting in the red overwhelming TPEF. These reasons lead to a moderate colocalization between the THG and TPEF signals in the pharynx region of the worm. Each figure shows a maximum intensity projection of 10 slice images. The “maximum intensity projection” creates an output image each of whose pixels contains the maximum value over all images in the stack (consisting of 10 slices in our case) at the particular pixel location.

Once the lipid existence was confirmed on the muscles, our experiments could proceed to the quantification of the THG signal. The part of the *C. elegans* that is chosen for quantification is the head region, because, as mentioned earlier, it is the region where intestinal lipids are avoided and also it is an area full of strong muscles emanating high SHG signal.

The THG signal quantification requires the setting of a threshold on the obtained normalized slice images. Regions generating high levels of nonlinear signal, which are mainly corresponding to lipid droplets, are solely detected and isolated. Processing of images and thresholding is performed by using Image J. Normalized 8-bit slice images of the sample are thresholded using a constant threshold value. Only the highest 23.5% of the THG signals is quantified in a way that the generated stack of binary images represents exclusively the lipid droplets in the muscles (ectopic fat), while any other signals from the contour or the mouth and the lumen are either excluded or eliminated. Lipid content is measured by calculating the total pixel area of detected regions for all optical planes covering the total sample volume. Figure 3 shows THG images recorded from the pharyngeal region of 1-day-old (Fig. 3a) and 9-day-old (Fig. 3d) wild-type *C. elegans* samples. In the same graph, the six thresholded binary central slices of THG corresponding to 1-day young (Fig. 3c) and 9-day-old (Fig. 3f) N2 *C. elegans* are depicted. Their z-projection is presented by Figures 3b and 3e, respectively.

The total sum of the detected areas (in pixels) is calculated as a representative index of the total lipid content within the examined part of the pharynx region. Total lipid particle area measurements of these two different samples are compared by one sample t-test (SPSS, IBM Corp.).

The total volume of the ectopic fat of each animal is calculated and averaged over a number of 18 animals for each age. Figure 4 depicts the mean total lipid content area in the head muscles of wild type animals of 1-day and 9-day old. The graph reveals the increase in the ectopic fat content along with the age progress of the animals. This difference is statistical significant ($P < 0.005$). It is already reported that *C. elegans* adult hermaphrodite animals display an age-related increase in body size (length, width, and volume)

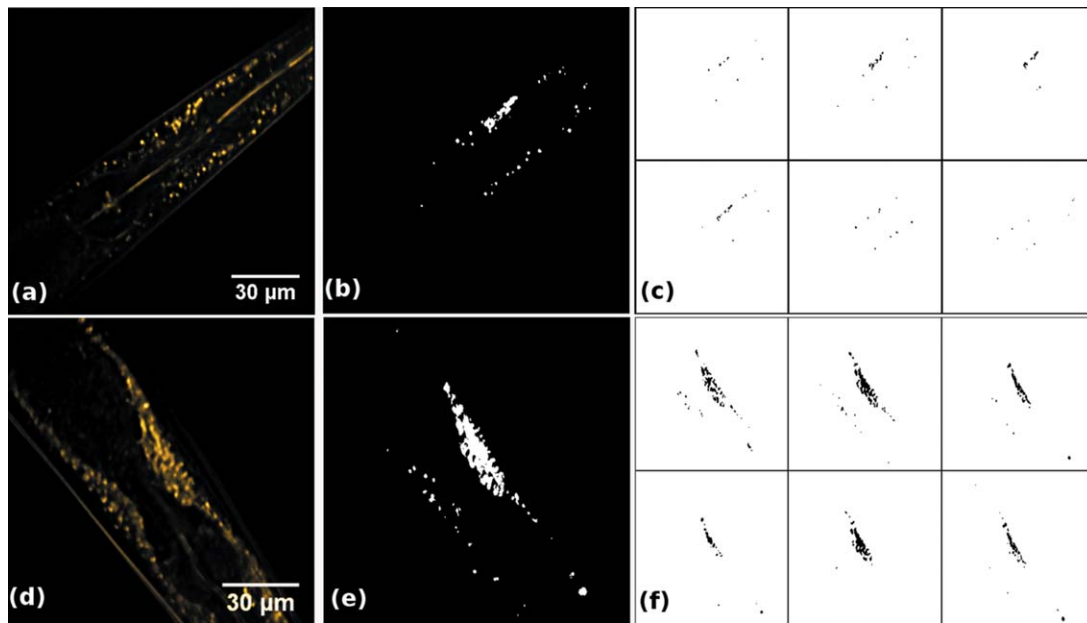


Fig. 3. THG images of wild-type (N2) animals (a) 1-day and (d) 9-day old, respectively. Z-projection of all the binary thresholded slices of (b) 1-day-old and (e) 9-day-old animals. The binary thresholded

sequence of slices of THG images corresponding to (c) 1-day-old and (f) 9-day-old worms. [Color figure can be viewed in the online issue, which is available at wileyonlinelibrary.com.]

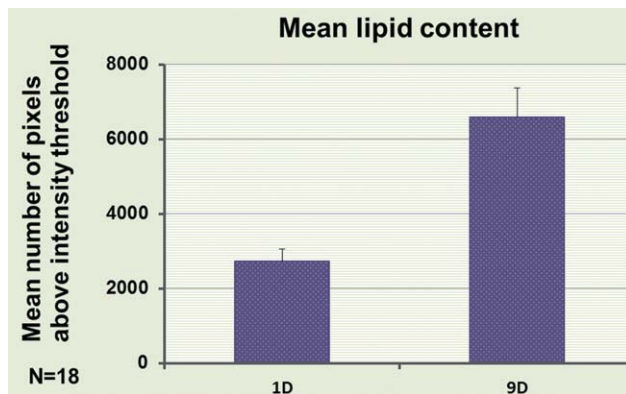


Fig. 4. Quantification of the mean total lipid area of 1-day-old and 9-day old wild-type (N2) animals, normalized with respect to the body size ($n = 18$, error bars denote the standard error of the mean SEM). [Color figure can be viewed in the online issue, which is available at wileyonlinelibrary.com.]

between day 3 to day 14 (Bolanowski et al., 1981; Croll et al., 1977). For our experiments, only the lipids between the two bulbs are measured and quantified. All the areas of the young and the old animals were measured giving a 1.38:1 (old/young) volume ratio, according to which the fat content was normalized. The difference in the lipid area between the young and the old animals is still significant.

These results indicate that THG modality could be used as a new nondestructive label-free diagnostic tool for the ectopic fat visualization and quantification in lipid biology research. By employing this technique, no external dyes are needed for staining the lipids. Moreover, complementary information can be obtained

related to the anatomy and morphology of the muscles via the simultaneously detection of SHG signals.

CONCLUSIONS

Nonlinear imaging microscopy modalities are well-established techniques for the in vivo delineation and mapping of subcellular biological structures and processes. In this study, we show that THG can be used as a new diagnostic tool for the accurate visualization and quantification of ectopic fat accumulation in nonadipose tissues of *C. elegans* samples without the need of external dyes. We have achieved to visualize simultaneously the muscles and the lipid droplets distribution in the pharyngeal region of unstained wild-type *C. elegans* samples by employing SHG and THG imaging techniques. By performing quantification of the collected THG signals a significant increase in the ectopic fat accumulation in older animals was detected. Changes of fat distribution in elderly animals could lead to lipotoxic effects, contributing to the disruption of tissue function during aging (Hemdon et al., 2002). It is possible that free fatty acids (FFAs) or their metabolites trigger cell death or oxidative stress damaging cellular function (Furuno et al., 2001; Piro et al., 2002; Scorrano et al., 2001; Wrede et al., 2002). However, further studies are necessary to delineate the link between ectopic fat accumulation and the process of aging.

Multiphoton microscopes are now commercially available and they can be easily upgraded for the detection of additional nonlinear signals (SHG, THG). Nonlinear microscopes are flexible and easy to use systems. A single femtosecond laser beam is required for the achievement of the measurements (TPEF, SHG, and THG), in contrast to other more complicated label-free microscopy techniques such as CARS. These

advantages facilitate the widespread adoption of non-linear imaging microscopy and especially THG modality as a versatile, reliable, and easily accessible tool for lipid biology research

REFERENCES

- Aptel F, Olivier N, Deniset-Bessau A, Legeair JM, Plamann K, Schanne-Klein MC, Beaufreire E. 2010. Multimodal nonlinear imaging of the human cornea. *Invest Ophthalmol Vis Sci* 51:2459–2465.
- Ashrafi K, Chang FY, Watts JL, Fraser AG, Kamath RS, Ahringer J, Ruvkun G. 2003. Genome-wide RNAi analysis of *caenorhabditis elegans* fat regulatory genes. *Nature* 421:268–272.
- Aviles-Espinosa R, Santos S, Brodschelm A, Kaenders WG, Alonso-Ortega C, Artigas D, Loza-Alvarez P. 2010. Third-harmonic generation for the study of *caenorhabditis elegans* embryogenesis. *J Biomed Opt* 15:046020–046020-7.
- Bolanowski MA, Russell RL, Jacobson LA. 1981. Quantitative measures of aging in the nematode *caenorhabditis elegans*. I. Population and longitudinal studies of two behavioral parameters. *Mech Ageing Dev* 15:279–295.
- Brooks KK, Liang B, Watts JL. 2009. The influence of bacterial diet on fat storage in *C. Elegans*. *PLoS One* 4:e7545.
- Cheng TX, Xie XS. 2004. Coherent anti-stokes Raman scattering microscopy: Instrumentation, theory, and applications. *J Phys Chem B* 108:827–840.
- Cox G, Kable E, Jones A, Fraser I, Manconi F, Gorell M. 2003. 3-dimensional imaging of collagen using second harmonic generation. *J Struct Biol* 141:53–62.
- Croll NA, Smith JM, Zuckerman BM. 1977. The aging process of the nematode *caenorhabditis elegans* in bacterial and axenic culture. *Exp Aging Res* 3:175–189.
- Débarre D, Supatto W, Pena AM, Fabre A, Tordjmann T, Combettes L, Schanne-Klein MC, Beaufreire E. 2006. Imaging lipid bodies in cells and tissues using third-harmonic generation microscopy. *Nat Meth* 3:47–53.
- Dombeck DA, Kasischke KA, Vishwasrao HD, Ingelsson M, Hyman BT, Webb WW. 2003. Uniform polarity microtubule assemblies imaged in native brain tissue by second-harmonic generation microscopy. *Proc Natl Acad Sci USA* 100:7081–7086.
- Filippidis G, Gualda EJ, Mari M, Troulinaki K, Fotakis C, Taverarakis N. 2009. In vivo imaging of cell morphology and cellular processes in *caenorhabditis elegans*, using non-linear phenomena. *Micron* 40:876–880.
- Furuno T, Kanno T, Arita K, Asami M, Utsumi T, Doi Y, Inoue M, Utsumi K. 2001. Roles of long chain fatty acids and carnitine in mitochondrial membrane permeability transition. *Biochem Pharmacol* 68:1037–1046.
- Greenspan P, Fowler SD. 1985. Spectrofluorometric studies of the lipid probe, Nile red. *J Lipid Res* 26:781–789.
- Gualda EJ, Philippidis G, Voglis G, Mari M, Fotakis C, Tavernarakis N. 2008. In vivo imaging of cellular structures in *caenorhabditis elegans* by combined TPEF, SHG and THG microscopy. *J Microsc* 229:141–150.
- Hellerer T, Axaeng C, Brackman C, Hillertz P, Pilon M, Enejder A. 2007. Monitoring of lipid storage in *caenorhabditis elegans* using coherent anti-stokes Raman scattering (CARS) microscopy. *Proc Natl Acad Sci USA* 104:14658–14663.
- Hemdon LA, Schmeissner PJ, Dudaronek JM, Brown PA, Listner KM, Sakano Y, Paupard MC, Hall DH, Driscoll M. 2002. Stochastic and genetic factors influence tissue-specific decline in ageing *C. elegans*. *Nature* 419:808–814.
- Kyvelidou C, Tservelakis GJ, Philippidis G, Ranella A, Kleovoulou A, Fotakis C, Athanassakis I. 2011. Following the course of pre-implantation embryo patterning by non-linear microscopy. *J Struct Biol* 176:379–386.
- Lu FK, Ji M, Fu D, Ni X, Freudiger CW, Holtom G, Xie XS. 2012. Multicolor stimulated Raman scattering (SRS) microscopy. *Mol Phys* 110:1927–1932.
- Mak HY, Nelson L, Basson M, Johnson CD, Ruvkun G. 2006. Polygenic control of *caenorhabditis elegans* fat storage. *Nat Genet* 38:363–368.
- Olivier N, Luengo-Oroz MA, Duloquin L. 2010. Cell lineage reconstruction of early zebrafish embryos using label-free nonlinear microscopy. *Science* 329:967–971.
- Oron D, Yelin D, Tal E, Raz S, Fachima R, Silberberg Y. 2004. Depth-resolved structural imaging by third-harmonic generation microscopy. *J Struct Biol* 147:3–11.
- Pelagati VB, Adur J, De Thomaz A, Almeida DB, Baratti MO, Andrade LA, Bottcher-luiz F, Cesar CL. 2012. Harmonic optical microscopy and fluorescence lifetime imaging platform for multimodal imaging. *Microsc Res Tech* 75:1383–1394.
- Piro S, Anello M, Di Pietro C, Lizzio MN, Patan G, Rabuazzo AM, Vigneri R, Purrello M, Purrello F. 2002. Chronic exposure to free fatty acids or high glucose induces apoptosis in rat pancreatic islets: Possible role of oxidative stress. *Metabolism* 51:1340–1347.
- Potma EO, Jones DJ, Cheng JX, Xie XS, Ye J. 2002. High-sensitivity coherent anti-stokes Raman microscopy with two tightly synchronized picosecond lasers. *Opt Lett* 27:1168–1170.
- Rehnberg M, Krombach F, Pohl U, Dietzel S. 2011. Label-free 3D visualization of cellular and tissue structures in intact muscle with second and third harmonic generation microscopy. *PLoS One* 6:e28237.
- Scorrano L, Penzo D, Petronilli V, Pagano F, Bernardi P. 2001. Arachidonic acid causes cell death through the mitochondrial permeability transition: Implications for tumor necrosis factor α apoptotic signaling. *J Biol Chem* 276:12035–12040.
- Tservelakis GJ, Philippidis G, Krmpot AJ. 2010. Imaging *caenorhabditis elegans* embryogenesis by third-harmonic generation microscopy. *Micron* 41:444–447.
- Tservelakis GJ, Philippidis G, Megalou E, Fotakis C, Tavernarakis N. 2011. Cell tracking in live *caenorhabditis elegans* embryos via third harmonic generation imaging microscopy measurements. *J Biomed Opt* 16:046019.
- Tservelakis GJ, Megalou E, Philippidis G, Petanidou B, Fotakis C, Tavernarakis N. 2014. Label-free imaging of lipid depositions in *C. Elegans* using third-harmonic generation microscopy. *PLoS One* 9:e84431.
- Vancoppenolle B, Claeys M, Borgonie G, Tytgat T, Coomans A. 2000. Evaluation of fixation methods for ultrastructural study of *caenorhabditis elegans* embryos. *Microsc Res Tech* 49:212–216.
- Wang MC, Min W, Freudiger CW, Ruvkun G, Xie XS. 2011. RNAi screening for fat regulatory genes with SRS microscopy. *Nat Meth* 8:135–138.
- Watts J, Browse J. 2002. Genetic dissection of polyunsaturated fatty acid synthesis in *caenorhabditis elegans*. *Proc Natl Acad Sci USA* 99:5854–5859.
- Watts J, Browse J. 2006. Dietary manipulation implicates lipid signaling in the regulation of germ cell maintenance in *C. Elegans*. *Dev Biol* 202:381–392.
- Witte S, Negrean A, Lodder JC, de Kock CPJ, Testa-Silva G, Mansvelder HD, Groot ML. 2011. Label free live brain imaging and targeted patching with third-harmonic generation microscopy. *Proc Natl Acad Sci USA* 108:5970–5975. P
- Wrede CE, Dickson LM, Linghor MK, Briaud I, Rhodes CJ. 2002. Protein kinase B/akt fatty acid induced apoptosis in pancreatic β -cells (INS-1). *J Biol Chem* 277:49676–49684.
- Zhuo S, Yan J, Chen G, Shi H, Zhu X, Lu J, Chen J, Xie S. 2012. Label-free imaging of basement membranes differentiates normal, precancerous and cancerous colonic tissues by second-harmonic generation microscopy. *PLoS One* 7:e38655.
- Zimmerley M, Mahou P, Débarre D, Schanne-Klein MC, Beaufreire E. 2013. Probing ordered assemblies with polarized third-harmonic generation microscopy. *Phys Rev X* 3:011002.1.